Journal of Alloys and Compounds 509 (2011) 3160–3165

Contents lists available at ScienceDirect

Journal of Alloys and Compounds

journal homepage: www.elsevier.com/locate/jallcom

Blue-yellow photoluminescence from $Ce^{3+} \rightarrow Dy^{3+}$ energy transfer in $HfO_2:Ce^{3+}:Dy^{3+}$ films deposited by ultrasonic spray pyrolysis

R. Martínez-Martínez[a], A.C. Lira[b], A. Speghini[c], C. Falcony[d,1], U. Caldiño[d,*]

[a] Instituto de Física y Matemáticas, Universidad Tecnológica de la Mixteca, Carretera a Acatlima Km. 2.5, Huajuapan de León, Oaxaca 69000, Mexico
[b] Unidad Académica Profesional Nezahualcóyotl, Universidad Autónoma del Estado de Mexico, Av. Bordo de Xochiaca s/n, Nezahualcóyotl, Estado de Mexico 57000,Mexico
[c] DiSTeMeV, Università di Verona, and INSTM, UdR Verona, Via Della Pieve 70, I-37029 San Floriano (Verona), Italy
[d] Departamento de Física, Universidad Autónoma Metropolitana-Iztapalapa, P.O. Box 55-534, Mexico, D.F. 09340, Mexico

ARTICLE INFO

Article history:
Received 20 July 2010
Received in revised form
25 November 2010
Accepted 25 November 2010
Available online 13 December 2010

PACS:
78.66.Nk
81.15.Rs
78.55.Hx

Keywords:
HfO_2
Ce^{3+}
Dy^{3+}
Films
Spray pyrolysis
Photoluminescence
Nonradiative energy transfer
Energy transfer efficiency

ABSTRACT

HfO_2 films codoped with Ce^{3+} and several concentrations of Dy^{3+} have been processed by the ultrasonic spray pyrolysis technique. Emissions from Dy^{3+} ions centred at 480 and 575 nm associated with the $^4F_{9/2} \rightarrow {}^6H_{15/2}$ and $^4F_{9/2} \rightarrow {}^6H_{13/2}$ transitions, respectively, have been observed upon UV excitation via a non-radiative energy transfer from Ce^{3+} to Dy^{3+} ions. Such energy transfer via an electric dipole–quadrupole interaction appears to be the most probable transfer mechanism. The efficiency of this transfer increases up to $86 \pm 3\%$ for the film with the highest Dy^{3+} content (1.9 ± 0.1 at.% as measured from EDS). The possibility of achieving the coordinates of ideal white light with increasing the concentration of dysprosium is demonstrated.

1. Introduction

Nowadays, the processing of white light emitting materials is of relevant interest to the optoelectronic industry. Several devices like plasma display panels [1], high brightness white light led technology based lighting systems, upconversion lasers and fiber amplifiers for optical communication [2] have been promoted using the photoluminescence properties of rare earth and transition metal ion-doped phosphors. The white light generation can be achieved by mixing of blue, green, yellow and red emissions from phosphors containing rare earth and transition metal ions [3]. Recently white light emission upon UV excitation was reported in $CeCl_3/TbCl_3/MnCl_2$ doped hafnium oxide films through an efficient sensitization of Tb^{3+} and Mn^{2+} ions by Ce^{3+} ions [4]. White light emission has been also attained in $Ca_3Y_2Si_3O_{12}$ [5] and Li_2CaGeO_4 [6] phosphors and oxyfluoride glass ceramics [7,8] codoped with Ce^{3+} and Dy^{3+} ions. In these materials white emission is originated from dysprosium through the mixture of its blue ($^4F_{9/2} \rightarrow {}^6H_{15/2}$) and yellow ($^4F_{9/2} \rightarrow {}^6H_{13/2}$) emissions, which are significantly enhanced through an efficient Dy^{3+} sensitization by Ce^{3+} ions excited at UV wavelengths. Ce^{3+} ions exhibit broad absorption bands in the UV, so that they can be easily excited by AlGaN/GaN-based LEDs [4]. The intense broad absorption band of Ce^{3+} ions is a consequence of their $4f \rightarrow 5d$ parity allowed electric dipole transitions, so that in co-doped materials such ions act as good sensitizers, transferring a part of their excitation energy to activator ions such as Tb^{3+} [4,9–11], Mn^{2+} [10–15] and Dy^{3+} [5–8,11].

The study of luminescent materials based on hafnium oxide (HfO_2) has attracted considerable attention, since it is a compound with a lot of possible technological applications because of its excellent physical and chemical properties, such as its high melting point

* Corresponding author.
E-mail address: cald@xanum.uam.mx (U. Caldiño).
[1] On leave from Centro de Investigaciones del IPN, Departamento de Física, 07000 México, DF, México.

0925-8388/$ – see front matter © 2010 Elsevier B.V. All rights reserved.
doi:10.1016/j.jallcom.2010.11.203

and high chemical stability. Its high dielectric constant and insulating properties [16] allow its application as a dielectric material with relatively high refractive index and wide band gap, as well in the field of optical coatings and metal-oxide semiconductor devices of the next generation [17]. HfO_2 films have been used as sensors to detect CO gas [18], and sensing characteristics to propane of these films synthesized by the ultrasonic spray pyrolysis (USP) technique were recently studied [19]. HfO_2 can also be used for protective coatings due its thermal stability and hardness near to diamond in its tetragonal phase [20]. The large energy gap and low phonon frequencies of the HfO_2 [21] makes it appropriate as host material to incorporate rare earth ions, such as Ce^{3+} [22], Er^{3+}[23], Tb^{3+} [24] and Eu^{3+} [25], as well as Mn^{2+}[26] and Sm^{3+} [27] ions, which emit within their own energy levels.

According to all these perspectives above mentioned and the importance of finding efficient luminescent materials for the design of phosphors as white light sources based on hafnium oxide, in this investigation an exhaustive analysis of the blue-yellow photoluminescence of HfO_2:Ce^{3+}:Dy^{3+} films synthesized by the UPS technique is presented. Moreover, this technique has demonstrated to be a very efficient way to synthesize luminescent films [13,15].

2. Experimental

Films of HfO_2 doped with only Dy^{3+} ions, and doubly doped with Ce^{3+} and Dy^{3+} ions were prepared using a low-cost process known as ultrasonic spray pyrolysis technique. In this technique, raw materials are mixed in a solvent, and then sprayed on a heated surface, where the constituents react to form a chemical compound. The detailed preparation of the spray solution is described elsewhere [10,13]. HfO_2:Ce^{3+}, HfO_2:Dy^{3+} and HfO_2:Ce^{3+}:Dy^{3+} films were deposited onto Corning 7059 glass slides used as substrates. The films were prepared using a spray solution of hafnium dichlororide oxide octahydrate (Aldrich Chemical Co, 99.99 + %) dissolved in deionised water (18 MΩ cm^{-1}). Cerium chloride heptahydrate and dysprosium chloride hexahydrate (Aldrich Chemical Co, 99.99 + %) were added as doping materials. The molar ratio of the spraying solution was 0.07. The substrate temperature during deposition was set at 300 °C. The carrier gas flow (filtered air) was 12 l min^{-1}. A 6 min deposition time was adjusted in order to obtain similar thicknesses for all the films studied. In the cerium or dysprosium singly doped films the $CeCl_3$ or $DyCl_3$ concentration in the spraying solution was 3 at.%. In the co-doped films the $CeCl_3$ concentration in the spraying solution was fixed at 3 at.%, varying only the $DyCl_3$ concentration (1.5, 3, 6 and 9 at.%). The crystalline structure of the films was analysed by X-ray diffractometry (XRD) using a 1.540 Å (Cu Kα) Siemens D5000 diffractometer, which was operated at 30 keV. The chemical composition of the films was measured using energy dispersive spectroscopy (EDS) with a Leica Cambridge Electron Microscope model Stereoscan 440 equipped with a beryllium window X-ray detector.

Photoluminescence and phosphorescence measurements were carried out using a Horiba Jobin–Yvon Fluorolog 3-22 spectrofluorometer.

The decay curves of the Ce^{3+} and Dy^{3+} emissions were recorded with 355 nm excitation of a pulsed YAG:Nd laser. A fiber optic probe was employed to collect the emission. The emitted light was dispersed by means of a half-meter monochromator equipped with a 150 lines/mm grating, and finally detected by a GaAs photomultiplier. The signal detected by the photomultiplier was then averaged and recorded by a digital oscilloscope. The very short decay times of the Ce^{3+} emission were obtained from the decay curves using a deconvolution procedure, which takes into account the shape and duration (about 8 ns) of the excitation pulse.

All the measurements were performed at room temperature.

3. Results and discussion

3.1. EDS and XRD measurements

The chemical composition of the studied films was determined by EDS. The values measured by EDS are listed in Table 1, which shows the relative atomic percentages of oxygen, chlorine, hafnium, cerium and dysprosium present in the films as a function of the $CeCl_3$ and $DyCl_3$ contents in the spraying solution. The studied films: HfO_2:$CeCl_3$(3 at.%), HfO_2:$DyCl_3$(3 at.%), HfO_2:$CeCl_3$(3 at.%):$DyCl_3$(1.5 at.%), HfO_2:$CeCl_3$(3 at.%):$DyCl_3$(3 at.%), HfO_2:$CeCl_3$(3 at.%):$DyCl_3$(6 at.%) and HfO_2:$CeCl_3$(3 at.%):$DyCl_3$ (9 at.%) will be referred to hereafter in terms of their Dy^{3+} concentration measured by EDS as HOC, HOD0.6, HOCD0.5, HOCD1.1, HOCD1.5 and HOCD1.9, respectively.

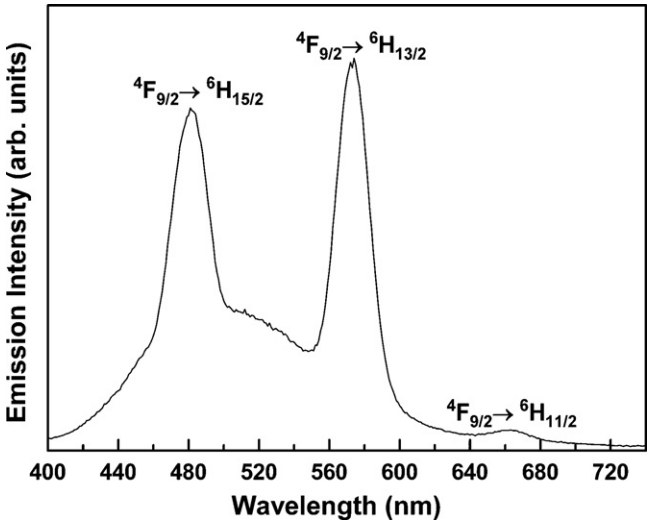

Fig. 1. Emission spectrum of the HOD0.6 film excited at 349 nm and recorded with a delay time of 0.01 ms.

X-ray diffraction patterns recorded for the films deposited at 300 °C exhibited a very broad band, and therefore they can be considered as predominantly amorphous.

An incorporation of chlorine ions might to be induced by the Ce^{3+} and/or Dy^{3+} ion substitution into Hf^{4+} cations in order to preserve the electrical neutrality in the trivalent ion doped HfO_2 film [22].

3.2. Photoluminescence of HfO_2:Dy^{3+}

The emission spectrum recorded for the HOD0.6 film excited at 349 nm, into the $^4M_{15/2}$,$^6P_{7/2}$ absorption band of Dy^{3+}, exhibits several bands associated with transitions from the $^4F_{9/2}$ level to the $^6H_{15/2}$, $^6H_{13/2}$ and $^6H_{11/2}$ multiplets, which are centred at 480 nm (blue), 575 nm (yellow) and 663 nm (red), respectively (Fig. 1). This emission spectrum was recorded with a delay time of 0.01 ms, so that the intrinsic emission of the HfO_2 host is substantially eliminated. Major contribution to intense, bright, yellow emission comes from the $^4F_{9/2}\rightarrow {}^6H_{13/2}$ transition. No emissions from the $^4M_{15/2}$,$^6P_{7/2}$ levels is observed, which suggests that Dy^{3+} ions depopulate nonradiatively from these levels to the $^4F_{9/2}$ emitting level. This level is separated from the next lower lying level ($^6F_{1/2}$) by about 7200 cm^{-1}, which makes the multiphonon relaxation negligible. It appears that only radiative transitions and relaxation by non-radiative energy transfer could be depopulating the $^4F_{9/2}$ level.

The excitation spectrum of the HOD0.6 film monitored at 575 nm, into the $^4F_{9/2}\rightarrow {}^6H_{13/2}$ emission transition, consists of Dy^{3+} excitation bands corresponding to transitions from the $^6H_{15/2}(4f^9)$ ground state to higher energy states of the $4f^9$ configuration (Fig. 2), which are centred at 324 nm ($^6H_{15/2}\rightarrow {}^4L_{19/2}$), 350 nm ($^6H_{15/2}\rightarrow {}^4M_{15/2}$,$^6P_{7/2}$), 364 nm ($^6H_{15/2}\rightarrow {}^4I_{11/2}$), 385 nm ($^6H_{15/2}\rightarrow {}^4K_{17/2}$,$^4M_{19/2,21/2}$,$^4I_{13/2}$, $^4F_{7/2}$), 424 nm ($^6H_{15/2}\rightarrow {}^4G_{11/2}$), 450 nm ($^6H_{15/2}\rightarrow {}^4I_{15/2}$) and 467 nm ($^6H_{15/2}\rightarrow {}^4F_{9/2}$).

The decay curve of the ($^4F_{9/2}\rightarrow {}^6H_{13/2}$) yellow emission of Dy^{3+} in the HOD0.6 film was recorded at 575 nm with Ce^{3+} excitation at 355 nm. It is non-exponential, so that its average decay time τ_{av} was obtained through the expression:

$$\tau_{av} = \frac{\int t\, I(t)\mathrm{d}t}{\int I(t)\mathrm{d}t} \quad (1)$$

where $I(t)$ is the emission intensity at time t. The τ_{av} value obtained for the Dy^{3+} yellow emission was 22 ± 1 μs, see Fig. 3.

Table 1
Atomic percent content of oxygen, chlorine, hafnium, cerium and dysprosium in the $CeCl_3$ and $DyCl_3$ doped HfO_2 films as measured by EDS.

Film	Solution content (at.%)		Chemical composition (at.%)				
	$CeCl_3$	$DyCl_3$	O^{2-}	Cl^-	Hf^{4+}	Ce^{3+}	Dy^{3+}
HOC	3	–	60.8 ± 0.6	10.5 ± 0.3	28.0 ± 0.3	0.7 ± 0.1	–
HOD0.6	–	3	60.9 ± 0.5	10.2 ± 0.3	28.3 ± 0.3	–	0.6 ± 0.1
HOCD0.5	3	1.5	62.8 ± 0.3	10.0 ± 0.2	25.8 ± 0.2	0.9 ± 0.1	0.5 ± 0.1
HOCD1.1	3	3.0	62.0 ± 0.2	9.6 ± 0.1	26.4 ± 0.1	0.9 ± 0.1	1.1 ± 0.1
HOCD1.5	3	6.0	59.8 ± 1.0	10.8 ± 0.3	27.0 ± 0.3	0.9 ± 0.1	1.5 ± 0.3
HOCD1.9	3	9.0	61.3 ± 0.3	11.8 ± 0.3	24.2 ± 0.2	0.8 ± 0.1	1.9 ± 0.1

3.3. Photoluminescence of $HfO_2:Ce^{3+}:Dy^{3+}$

Fig. 4(a) shows emission spectra of the HOC, HOCD0.5, HOCD1.1, HOCD1.5 and HOCD1.9 films excited with 280 nm wavelength, within the Ce^{3+} $4f \rightarrow 5d$ absorption transition. All these spectra, which have been recorded in the same experimental conditions for comparison, exhibit the blue broad band associated with the $5d^1 \rightarrow 4f^1$ transition of Ce^{3+} ions [22]. The emission spectra of the cerium and dysprosium codoped films exhibit, in addition to the Ce^{3+} emission band, the $^4F_{9/2} \rightarrow {}^6H_{15/2}$ and $^4F_{9/2} \rightarrow {}^6H_{13/2}$ emissions of Dy^{3+}. The addition of Dy^{3+} ions in the Ce^{3+} doped film causes a strong decrease of the cerium overall emission, and moreover, as the Dy^{3+} content is increased, a quenching of the Ce^{3+} emission intensity correlates with an increasing of the Dy^{3+} emission intensity and it reaches a maximum for the HOCD1.1 film (see Fig. 4(b), which shows the normalized spectra to the Ce^{3+} emission band). These facts represent evidence that energy transfer from Ce^{3+} to Dy^{3+} ions occurs through a nonradiative process. For the film with the highest content of Dy^{3+} (HOCD1.9) the Dy^{3+} emission is concentration quenched. Moreover, as the Dy^{3+} concentration is increased, the Ce^{3+} emission peak is blue shifted by 14 nm from 389 nm for the HOCD0.5 film to 375 nm for the HOCD1.9 film. This blue shift can be attributed to the Ce^{3+} split ground state, into their $^2F_{5/2}$ and $^2F_{7/2}$

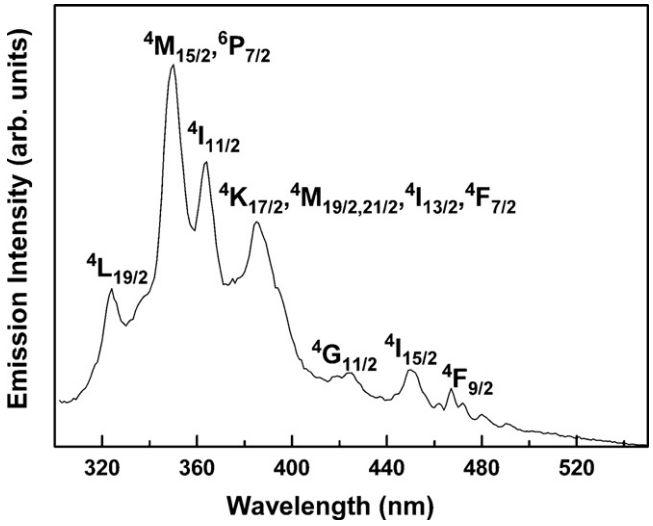

Fig. 2. Excitation spectrum of the HOD0.6 film monitored at 575 nm.

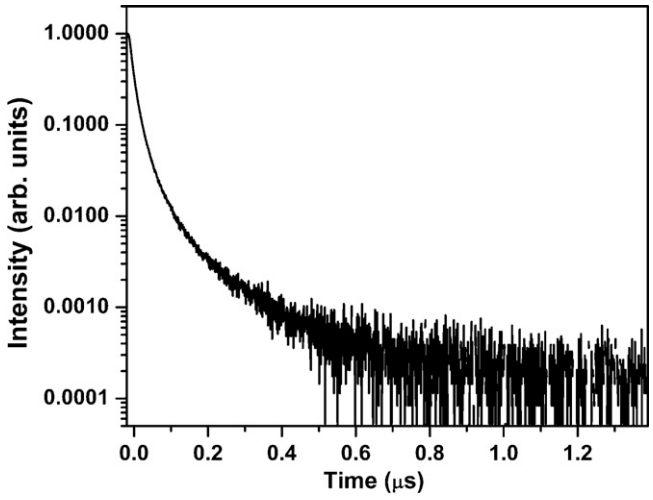

Fig. 3. Decay time curve of Dy^{3+} emission (λ_{em} = 575 nm) for the HOD0.6 film excited at 355 nm.

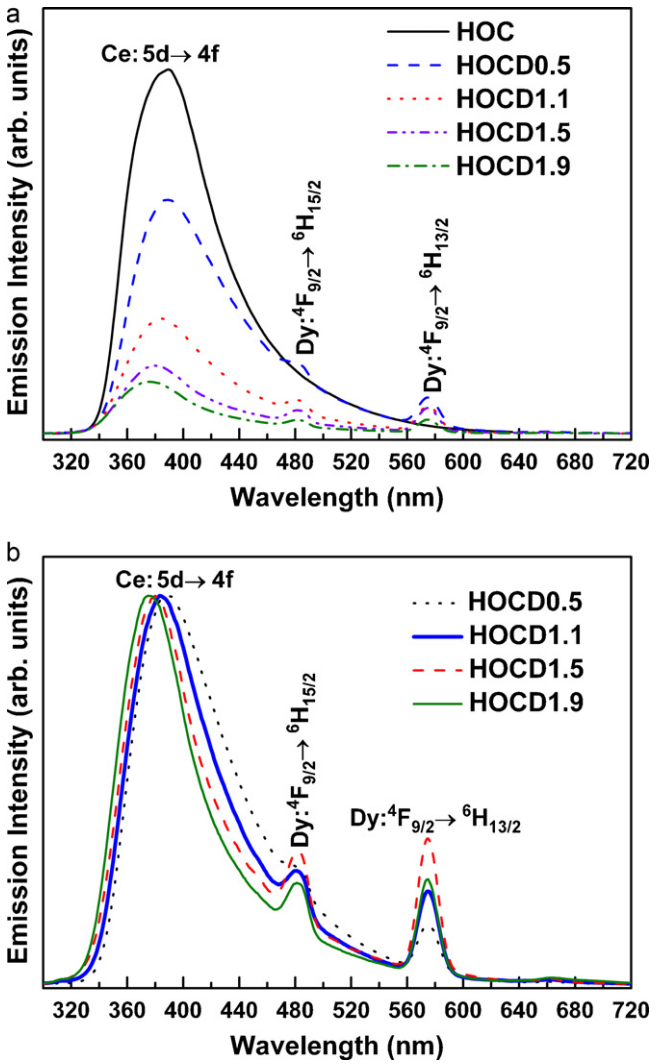

Fig. 4. Emission spectra of HfO_2 singly doped with Ce^{3+} ions and codoped with Ce^{3+} and Dy^{3+} ions after 280 nm excitation (a) under the same experimental conditions and (b) normalized to the Ce^{3+} emission band.

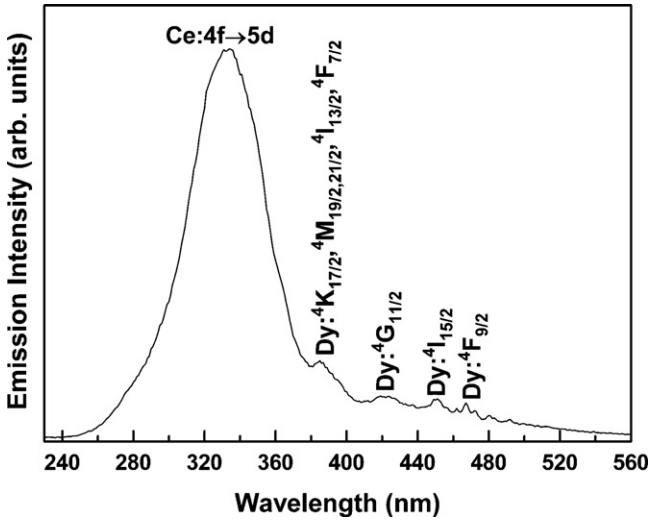

Fig. 5. Excitation spectrum of the HOCD0.5 film monitored at 575 nm.

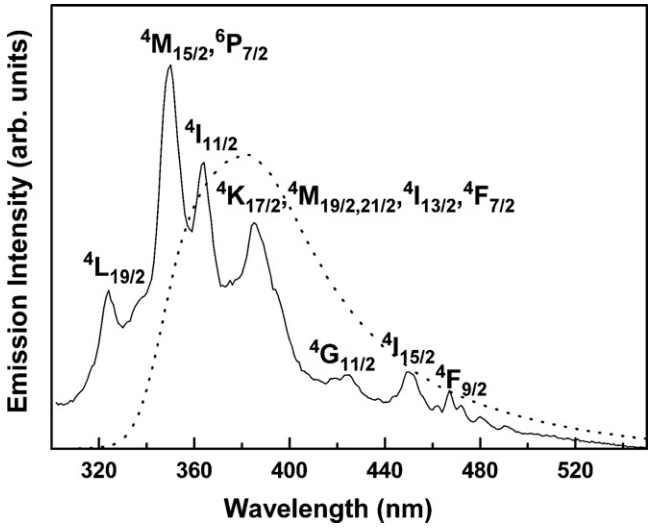

Fig. 6. Overlap region of Dy^{3+} absorption (excitation) transitions (solid line) and Ce^{3+} emission (dashed line). The Dy^{3+} excitation spectrum was taken from that recorded for the HOD0.6 film (Fig. 2).

components, so that the energy transfer through the $5d^1 \rightarrow {}^2F_{7/2}$ low-energy emission component might be even more efficient than that through the $5d^1 \rightarrow {}^2F_{5/2}$ high-energy emission component as the Dy^{3+} content is increased.

The excitation spectrum monitored at 575 nm (inside the $^4F_{9/2} \rightarrow {}^6H_{13/2}$ emission transition of Dy^{3+}) exhibits, in addition to the ($^6H_{15/2} \rightarrow {}^4K_{17/2}$,$^4M_{19/2,21/2}$,$^4I_{13/2}$,$^4F_{7/2}$, $^6H_{15/2} \rightarrow {}^4G_{11/2}$, $^6H_{15/2} \rightarrow {}^4I_{15/2}$ and $^6H_{15/2} \rightarrow {}^4F_{9/2}$) Dy^{3+} absorption (excitation) transitions, a broad band in the 260–380 nm region, which is similar to the 4f→5d Ce^{3+} absorption (excitation) band observed in the excitation spectrum of a HfO_2 film doped with 1.9 at.% of Ce^{3+} [22]. This excitation spectrum is shown in Fig. 5 for the HOCD0.5 film. The presence of the Ce^{3+} band in the Dy^{3+} excitation spectrum suggests an energy transfer from Ce^{3+} to Dy^{3+} ions, which is expected to occur considering that the Ce^{3+} emission overlaps the $^6H_{15/2} \rightarrow {}^4L_{19/2}$, $^6H_{15/2} \rightarrow {}^4M_{15/2}$,$^6P_{7/2}$, $^6H_{15/2} \rightarrow {}^4I_{11/2}$, $^6H_{15/2} \rightarrow {}^4K_{17/2}$,$^4M_{19/2,21/2}$,$^4I_{13/2}$,$^4F_{7/2}$, $^6H_{15/2} \rightarrow {}^4G_{11/2}$, $^6H_{15/2} \rightarrow {}^4I_{15/2}$ and $^6H_{15/2} \rightarrow {}^4F_{9/2}$ absorption (excitation) transitions of Dy^{3+} (Fig. 6).

Lifetime measurements of the Ce^{3+} emission in the HfO_2 films Ce^{3+} doped singly (HOC) and Ce^{3+}/Dy^{3+} codoped (HOCD0.5, HOCD1.1, HOCD1.5 and HOCD1.9) were performed monitoring at

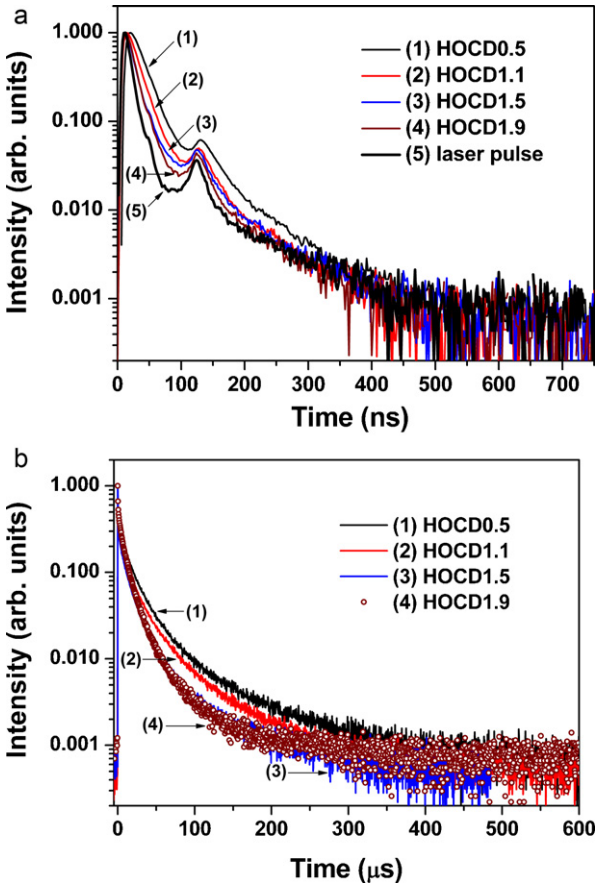

Fig. 7. Decay curves of (a) Ce^{3+} emission (λ_{em} = 440 nm) and (b) Dy^{3+} emission (λ_{em} = 575 nm) for the HOC0.5, HCD1.1, HCD1.5, HCD1.9 films excited at 355 nm.

440 nm with Ce^{3+} excitation at 355 nm. Fig. 7(a) shows the Ce^{3+} emission decay time curves recorded for the Ce^{3+} and Dy^{3+} codoped films. Such decay time curves appear to be non-exponential due to the energy transfer from Ce^{3+} to Dy^{3+} ions. In the HOCD0.5 film the Ce^{3+} emission decay time value, once deconvoluted from the laser excitation pulse profile, resulted to be around 8.0 ± 0.5 ns involving a shortening of the Ce^{3+} emission decay time with respect to the one (around 11.6 ± 0.5 ns) measured for the HOC film or that (14 ns [15]) previously measured for a HfO_2:Ce^{3+}(1.9 at.%) film. From Fig. 7(a) it can also be noticed that the Ce^{3+} emission decay is steeper with increasing of Dy^{3+} content. Considering that the laser excitation pulse has a temporal width of about 8 ns, then the decay time curves of the Ce^{3+} emission in the films with higher Dy^{3+} concentration (HOCD1.1, HOCD1.5 and HOCD1.9) might well be shorter than 8 ns. Anyway, the increase in the Ce^{3+} emission decay rate on co-doping with dysprosium can be attributed to nonradiative energy transfer from Ce^{3+} to Dy^{3+} ions.

Lifetime measurements of the $^4F_{9/2} \rightarrow {}^6H_{13/2}$ yellow emission of Dy^{3+} were carried out with Ce^{3+} excitation at 355 nm. The decay time curve of this emission is non-exponential, so that its average decay time τ_{av} was obtained through Eq. (1). The τ_{av} value decreases with increasing the Dy^{3+} concentration from 22 ± 1 μs (HOCD0.5 film) to 13 ± 1 μs (HOCD1.9 film), see Fig. 7(b). The lifetime value measured for the HOCD0.5 film is the same as the one measured for the Dy^{3+} singly doped film (HOD0.6), so that the same decay times are obtained for the Dy^{3+} yellow emission under direct excitation and through Ce^{3+} ions. This fact suggests the absence of $Ce^{3+} \leftarrow Dy^{3+}$ back energy transfer as expected from the vanishing overlap between Dy^{3+} emissions and Ce^{3+} absorptions.

From the very short and long lifetimes measured for the Ce^{3+} and Dy^{3+} emissions, respectively, it is expected that the energy transfer from Ce^{3+} to Dy^{3+} ions could occur through an electric dipole–quadrupole (d–q) interaction mechanism.

Assuming an electric d–q interaction mechanism, the transfer rate W_{dq} between sensitizer (Ce^{3+}) and activator (Dy^{3+}) ions is given by [28]:

$$W_{dq} = \frac{3\hbar^4 c^4 f_q \lambda_s^2 Q_a}{4\pi n^4 \tau_s^o f_d R_{sa}^8} \Omega, \quad (2)$$

where $\Omega = \int [F_s(E)F_a(E)/E^4]dE$ is the spectral overlap integral between the normalised line-shape functions of the Ce^{3+} emission $F_s(E)$ and Dy^{3+} absorption $F_a(E)$, with E being the average energy of the overlapping transition. The meaning of the remaining symbols in Eq. (2) has been described elsewhere [9,15]. The Dy^{3+} integrated absorption coefficient Q_a ($\approx 1.2 \times 10^{-25}$ eV m^2) was estimated following the same procedure as that employed previously [9,12–15]. In the wavelength region of Ce^{3+} emission (330–540 nm) the f_d electric dipole oscillator strength of the Dy^{3+} is very low (2.5×10^{-6} [29]), since the Dy^{3+} transition is more or less forbidden as an electric dipole transition by the parity selection rule. The f_q electric quadrupole oscillator strength was estimated from its relation with f_d [28], $f_q = (a/\lambda_a)^2 f_d$, as the Dy^{3+} absorption transitions are quite weak to be recorded. Using $a \approx 1$ Å (radius of the Dy^{3+}) and $\lambda_{Dy} \approx 3800$ Å (wavelength of the absorbed light by the dysprosium in the cerium emission), and considering that the forbidden electric dipole transitions are weaker than the allowed ones by a factor of 10^{-4} to 10^{-5}, then the ratio f_q/f_d is 10^{-2} to 10^{-3} for the Dy^{3+}. The R_{sa} sensitizer–activator average interaction distance was estimated from the contents of Ce^{3+} and Dy^{3+} measured by EDS (see Table 2) assuming a random ion distribution. Using $n = 2.0$, and the values estimated for f_q/f_d, Q_a, $R_{sa} = (13.7 \pm 0.3–17.1 \pm 0.8$ Å) and Ω ($=6.9 \times 10^{-3}$ eV^{-5}), it is found that the $Ce^{3+} \rightarrow Dy^{3+}$ energy transfer rate increases from $4 \times 10^6 - 10^7$ s^{-1} in the HOCD0.5 film up to $2 \times 10^7 - 10^8$ s^{-1} in the HOCD1.9 film (see Table 2). Thus, the transfer rate in the film with the lowest Dy^{3+} content (HOCD0.5) is smaller than the rate of Ce^{3+} radiative emission ($1/\tau_s^o = 1 \times 10^8$ s^{-1}), but in the films with higher Dy^{3+} content the transfer rate becomes comparable or higher than the Ce^{3+} intrinsic decay rate.

For sake of comparison the transfer rate for an electric dipole–dipole (d–d) interaction mechanism, W_{dd}, was estimated from its relation with the W_{dq} rate [14]. The W_{dd} rate increases from 1×10^5 s^{-1} in the HOCD0.5 film up to 3×10^5 s^{-1} in the HOCD1.9 film, see Table 2, so that such rates are quite smaller than the Ce^{3+} radiative emission rate. Therefore, the $Ce^{3+} \rightarrow Dy^{3+}$ energy transfer through an electric d–q interaction mechanism appears to be more probable than that via an electric d–d interaction mechanism.

The η energy transfer efficiency from Ce^{3+} to Dy^{3+} ions can be estimated from the emission intensities of the Ce^{3+} in the presence (I_S) and absence (I_S^o) of the Dy^{3+} through the following relation [9]:

$$\eta = 1 - \frac{I_S}{I_S^o}. \quad (3)$$

Thus, the efficiency of $Ce^{3+} \rightarrow Dy^{3+}$ energy transfer was estimated using Eq. (3) and the cerium emission spectra shown in Fig. 4(a). Such efficiency increases from 29 ± 1% (HOCD0.5 film) up to 86 ± 3% (HOCD1.9 film), see Fig. 8 and Table 2. This efficiency tends to saturate at Dy^{3+} concentrations of around 1.9 at.%. The very low energy transfer efficiency measured for the

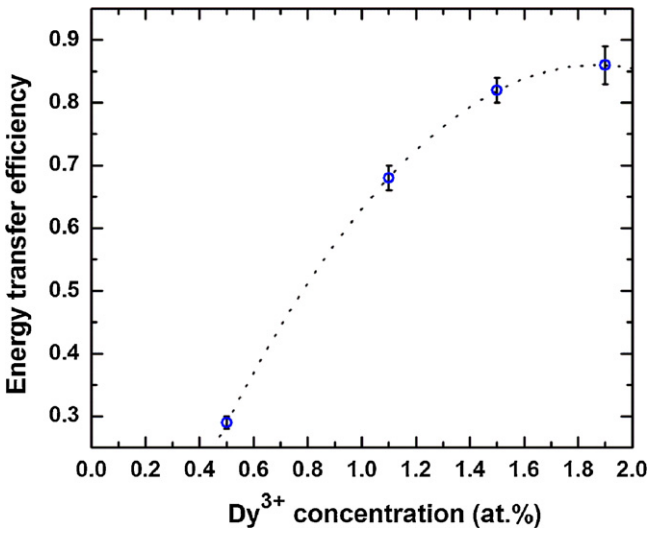

Fig. 8. Ce^{3+} to Dy^{3+} energy transfer efficiency as a function of dysprosium content. The dotted line is drawn to guide the eyes.

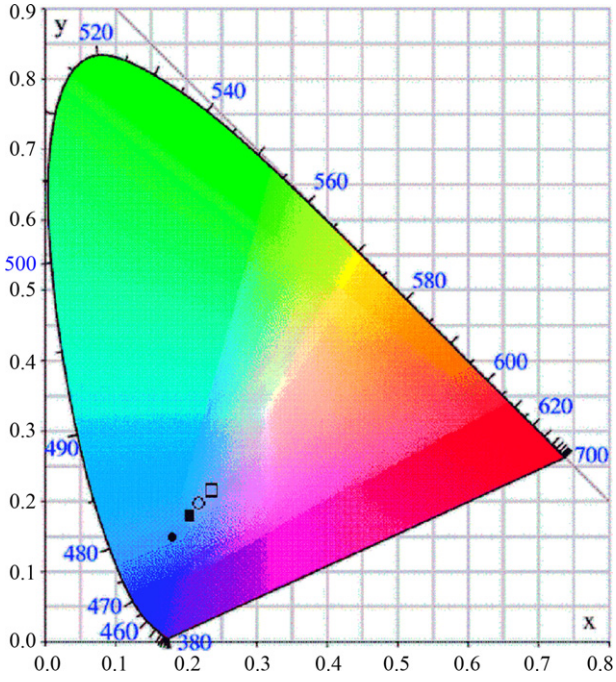

Fig. 9. Chromaticity coordinates characteristic of the emissions observed in the HOCD0.5 (solid circle symbol), HOCD1.1 (solid square symbol), HOCD1.5 (circle symbol) and HOCD1.9 (square symbol) films excited at 280 nm.

Table 2
R_{sa} average Ce^{3+}–Dy^{3+} interaction distances, W_{dd} and W_{dq} rates and η efficiencies of $Ce^{3+} \rightarrow Dy^{3+}$ energy transfer in the HOCD0.5, HOCD1.1, HOCD1.5 and HOCD1.9 films.

Film	R_{sa} (Å)	W_{dd}(s^{-1})	W_{dq} (s^{-1})	η(%)
HOCD0.5	17.1 ± 0.8	1×10^5	4×10^6–10^7	29 ± 1 31 ± 5[a]
HOCD1.1	15.2 ± 0.5	1×10^5	1×10^7–10^8	68 ± 2
HOCD1.5	14.2 ± 0.8	2×10^5	2×10^7–10^8	82 ± 2
HOCD1.9	13.7 ± 0.3	3×10^5	2×10^7–10^8	86 ± 3

[a] Energy transfer efficiency obtained from decay time measurements.

HOCD0.5 film is in agreement with a $Ce^{3+} \rightarrow Dy^{3+}$ energy transfer ($W_{dq} = 4 \times 10^6 - 10^7$) less probable than the Ce^{3+} intrinsic decay ($1/\tau_s^o = 1 \times 10^8\ s^{-1}$).

The transfer efficiency can also be obtained from data of the Ce^{3+} emission decay time in the presence (τ_{Ce}) and absence of the activators (τ_{Ce}^o) through the expression [9]:

$$\eta = 1 - \frac{\tau_{Ce}}{\tau_{Ce}^o}. \quad (4)$$

In the case of the HOCD0.5 film for which the Ce^{3+} emission decay time could be measured with our experimental set-up, there is a good agreement between energy transfer efficiencies obtained from decay time data ($\eta = 31 \pm 5$) and that determined from emission spectra. This good agreement suggests that $Ce^{3+} \rightarrow Dy^{3+}$ energy transfer through a radiative mechanism can be neglected, since radiative energy transfer does not cause any reduction in the sensitizer decay time [30].

The global emission generated by the HOCD0.5, HOCD1.1, HOCD1.5 and HOCD1.9 films (excited at 280 nm) was characterized by its chromaticity coordinates in a CIE diagram (Fig. 9), resulting in purplish blue light with chromaticity coordinates of (0.184, 0.153), (0.202, 0.170), (0.223, 0.198) and (0.231, 0.211), respectively. Thus, the global emission of the investigated films points in the direction of achieving the coordinates of ideal white light (0.333, 0.333) with increasing the concentration of dysprosium.

4. Conclusions

Blue-yellow emitting HfO_2:Ce^{3+}:Dy^{3+} films excited with UV radiation can be deposited at 300 °C by the ultrasonic spray pyrolysis technique. The blue emission is due to the Ce^{3+} ($5d^1 \rightarrow 4f^1$) and Dy^{3+} ($^4F_{9/2} \rightarrow {}^6H_{15/2}$) transitions and the yellow emission is associated with the $^4F_{9/2} \rightarrow {}^6H_{13/2}$ de-excitation of Dy^{3+} ions. The addition of $DyCl_3$ in the HfO_2:$CeCl_3$ film leads to a non-radiative energy transfer from Ce^{3+} to Dy^{3+} under Ce^{3+} excitation at 280 nm. The non-radiative character of this transfer is inferred from both a decrease of the Ce^{3+} overall emission and an increase in the decay rate of the Ce^{3+} emission, when the film is codoped with cerium and dysprosium. From spectroscopic data is inferred that Ce^{3+} to Dy^{3+} energy transfer via an electric dipole–quadrupole interaction appears to be the most probable transfer mechanism. The efficiency of this transfer is enhanced up to $86 \pm 3\%$ for the film with the highest Dy^{3+} content (HOCD1.9). The possibility of achieving the coordinates of ideal white light with increasing the concentration of dysprosium is demonstrated.

Acknowledgments

This work was supported by the CONACyT under project contract 78802-2F. The technical assistance of Z. Rivera, A. B. Soto and M. Guerrero is also acknowledged.

References

[1] P. Psuja, D. Hreniak, W. Strek, J. Nanomater (2007), Article Num. 81350.
[2] S. Tanabe, Glass Sci. Technol. 75 (Suppl. C1) (2002) 191.
[3] B. Moine, G. Bizarri, Sci. Mater, Eng. B-Solid State Mater. Adv. Technol. 105 (2003) 2.
[4] R. Martínez-Martínez, E. Álvarez, A. Speghini, C. Falcony, U. Caldiño, J. Mater. Res. 25 (2010) 484.
[5] V.R. Bandi, Y.T. Nien, I.G. Chen, J. Appl. Phys. 108 (2010) 023111.
[6] J.X. Meng, C.T. Yang, Q.Q. Chen, J. Lumin. 130 (2010) 1320.
[7] Q. Luo, X. Qiao, X. Fan, H. Yang, X. Zhang, S. Cui, L. Wang, G. Wang, J. Appl. Phys. 105 (2009) 043506.
[8] D.Q. Chen, Y.L. Yu, H. Lin, P. Huang, F.Y. Weng, Z.F. Shan, Y.S. Wang, Opt. Lett. 34 (2009) 2882.
[9] U. Caldiño, A. Speghini, M. Bettinelli, J. Phys.: Condens. Matter 19 (2006) 3499.
[10] R. Martínez-Martínez, A. Speghini, M. Bettinelli, C. Falcony, U. Caldiño, J. Lumin. 129 (2009) 1276.
[11] R.P. Sonekar, S.K. Omanwar, S.V. Moharil, P.L. Muthal, S.M. Dhopte, V.K. Kondawar, J. Lumin. 129 (2009) 624.
[12] U.G. Caldiño, J. Phys.: Condens. Matter 15 (2003) 3821.
[13] R. Martínez-Martínez, M. García-Hipólito, F. Ramos-Brito, J.L. Hernández-Pozos, U. Caldiño, C. Falcony, J. Phys.: Condens. Matter 17 (2005) 3647.
[14] U. Caldiño, J.L. Hernández-Pozos, C. Flores, A. Speghini, M. Bettinelli, J. Phys.: Condens. Matter 17 (2005) 7297.
[15] R. Martínez-Martínez, M. García, A. Speghini, M. Bettinelli, C. Falcony, U. Caldiño, J. Phys.: Condens. Matter 20 (2008) 395205.
[16] W. He, L. Zhang, D.S.H. Chan, B.J. Cho, IEEE Electron Device Lett. 30 (2009) 623.
[17] G.D. Wilk, R.M. Wallace, J.M. Anthony, J. Appl. Phys. 89 (2001) 5243.
[18] S. Capone, G. Leo, R. Rella, P. Siciliano, L. Vasanelli, M. Alvisi, L. Mirenghi, A. Rizzo, J. Vac. Sci. Technol. A 16 (1998) 3564.
[19] A. Avila-García, M. García-Hipólito, Sens. Actuators B 133 (2008) 302.
[20] H. Ibégazéne, S. Alpérine, C. Diot, J. Mater. Sci. 30 (1995) 938.
[21] X. Zhao, D. Vanderbilt, Phys. Rev. B65 (2002) 233106.
[22] M. García-Hipólito, U. Caldiño, O. Alvarez-Fragoso, M.A. Alvarez-Pérez, R. Martínez-Martínez, C. Falcony, Phys. Status Solidi A 204 (2007) 2355.
[23] M. Mattarelli, M. Montagna, F. Rossi, C. Tosello, N.D. Afify, M. Bettinelli, A. Speghini, C. Armellini, Y. Jestin, F. Rocca, S. Gialanella, Opt. Mater. 31 (2009) 1362.
[24] T. Sanada, M. Kawai, H. Nakashita, T. Matsumoto, N. Wada, K. Kojima, J. Ceram. Soc. Jpn. 116 (2008) 1265.
[25] R. Chora-Corella, M. Garcia-Hipolito, O. Alvarez-Fragoso, M.A. Alvarez-Perez, C. Falcony, Rev. Mex. Fis. 55 (2009) 226.
[26] M. Garcia-Hipolito, O. Alvarez-Fregoso, J. Guzman, E. Martinez, C. Falcony, Phys. Status Solidi a 201 (2004) R127.
[27] C. Chacón-Roa, J. Guzmán-Mendoza, M. Aguilar-Frutis, M. García-Hipólito, O. Alvarez-Fragoso, C. Falcony, J. Phys. D: Appl. Phys. 41 (2008) 015104.
[28] D.L. Dexter, J. Chem. Phys. 21 (1953) 836.
[29] M.A. Elïyashevich, Spectra of the Rare Earths, AEC translation 4403 (1961) p. 503.
[30] B. Henderson, G.F. Imbusch, Optical Spectroscopy of Inorganic Solids, Oxford Science Publications, Oxford, Clarendon, 1989.